Sensors and Actuators Reports 9 (2025) 100279

Contents lists available at ScienceDirect

Sensors and Actuators Reports

journal homepage: www.sciencedirect.com/journal/sensors-and-actuators-reports

Cortisol detection using a Long Period Fiber Grating Immunosensor coated with Graphene Oxide

Simone Soares [a,b,1], Ambra Giannetti [c,1], Flavio Esposito [d,1], Lucia Sansone [e,1], Anubhav Srivastava [d], Stefania Campopiano [d], Michele Giordano [e], Margarida Facão [b], Nuno F. Santos [b], Agostino Iadicicco [d,*], Carlos Marques [a,f,*], Francesco Chiavaioli [c,*]

[a] CICECO – Aveiro Institute of Materials, Physics Department, University of Aveiro, Aveiro 3810-193, Portugal
[b] I3 N and Physics Department, University of Aveiro, Aveiro 3810-193, Portugal
[c] Institute of Applied Physics "Nello Carrara", National Research Council of Italy (CNR), 50019 Sesto Fiorentino, Italy
[d] Department of Engineering, University of Naples "Parthenope", Centro Direzionale Isola C4, 80143 Napoli, Italy
[e] Institute for Polymers, Composites and Biomaterials, National Research Council of Italy (CNR), 80055 Portici, Italy
[f] Department of Physics, VSB – Technical University of Ostrava, Ostrava 70800, Czech Republic

ARTICLE INFO

Keywords:
Cortisol
Immunosensor
Graphene oxide
Long period fiber grating
Recirculating aquaculture systems

ABSTRACT

Recirculating Aquaculture Systems (RAS) have revolutionized the protein production sector in aquaculture, leading to significant growth and expansion of the industry. Despite the success of RAS in aquaculture, there are challenges related to stress in fish raised in these systems, which can impact their food intake, growth, and overall well-being. One of the major limitations in the aquaculture industry is the lack of smart sensors for real-time detection of stress hormones like cortisol, hindering our ability to understand and effectively manage the welfare of fish in these systems. In this work, a graphene oxide (GO) coated long period grating (LPG) was fabricated into a double-clad optical fiber (DCF) with W-shaped refractive index profile. The working point of the device was tuned to the mode transition region to enhance its sensitivity against outer medium changes. It was further integrated into a microfluidic system and the fiber surface was functionalized with specific anti-cortisol antibodies for the detection of cortisol. Finally, the performance of this immunosensor was evaluated for a cortisol concentration range of 0.01 ng/mL to 100 ng/mL, a wide working range of concentrations of relevant interest, achieving a limit of detection (LOD) of 0.06 ng/mL. Moreover, a selectivity test using testosterone and glucose as interfering substances was carried out.

1. Introduction

Different systems can be used for aquaculture growth production, including estuaries, ponds, cages, flow-through or recirculating aquaculture systems (RAS) [1]. In the last decade, RAS has become the new way of farming fish since it is the aquaculture production system that has increased rapidly. This system presents several advantages compared to traditional methods, including practicing in indoor tanks and high-density fish rearing in a controlled environment and in a more cost-efficient way [2,3]. Furthermore, with RAS it is possible to depurate water and reuse it in production (with 90 % recycled water) due to the presence of a series of treatment steps, allowing the raising of large quantities of fish in small volumes, the non-necessity for new sites and freshwater, as well as the reduction concerns over pollution [3,4].

Nonetheless, RAS are complex systems where small variations may result in sub-optimal conditions due to the interaction of fish biomass and water chemistry/quality. As a result, stress is induced, leading to reduced feed intake and may result in reduced growth performance or even mortality due to acute or chronic stress [5]. This is a major concern for the industry which needs to be addressed by the scientific community by monitoring critical parameters such as cortisol (stress hormone) in the water tanks to ensure fish well-being. Currently, no solutions are available for cortisol detection directly in the water. The traditional method is invasive and performed through blood sampling and analysis of blood plasma. This method is time-consuming, the results are only available long after the sampling and are influenced by the method

* Corresponding authors.
E-mail addresses: agostino.iadicicco@uniparthenope.it (A. Iadicicco), carlos.marques@ua.pt (C. Marques), f.chiavaioli@ifac.cnr.it (F. Chiavaioli).
[1] These authors contributed equally.

https://doi.org/10.1016/j.snr.2024.100279
Received 31 October 2024; Received in revised form 20 December 2024; Accepted 23 December 2024
Available online 25 December 2024

itself. Besides, it is rarely performed since it is expensive [6,7]. Subsequently, it was demonstrated for some fish that in response to stress, the cortisol release rate into the water of European sea bass increased and was correlated with the plasma cortisol concentrations from blood [6]. It should be noted that there are a lot of fish species produced in RAS where the cortisol levels can differ considerably from thousandths of ng/ml to hundreds of ng/ml. One recent study reported cortisol concentrations between 1 and 3 ng/mL (in normal conditions), analyzed in water samples collected from fish tanks, however, those values can change significantly in other environments [8]. Some works studied the cortisol levels of a few species of fish, including gilthead sea bream, sea bass, rainbow trout, and Senegalese sole, describing values between 5.65–26.3 ng/mL in healthy conditions and 24.2–114.6 ng/mL in stress conditions [9].

One of the major limitations of RAS is the lack of smart sensors for real-time detection of stress hormones like cortisol. The exploration of innovative technology can be a way to overcome this challenge. Therefore, the development of point-of-care (POC) biosensors for cortisol detection with fast response, *in situ* and non-invasive analysis can be the game changer since cortisol has proven to be an effective and reliable stress indicator, even in fish.

Optical fiber biosensors have demonstrated to possess unique features that make them a valid option for the detection of a specific analyte or molecule with high sensitivity, low limit of detection (LOD) and high specificity even when working with complex biological fluids [10–15]. With such devices combined with innovative materials in the form of nanofilms or nanostructures, it is possible to dramatically enhance the light-matter interaction leading to remarkably low LODs in the attomolar range [16,17].

Some works using optical fibers for cortisol detection are present in the literature. For instance, Leitão et al. [18] reported an immunosensor for cortisol detection based on tilted fiber Bragg grating (TFBG) supported by surface plasmon resonance (SPR). In this study, a standard single-mode silica optical fiber with 1 cm long TFBGs was coated with gold. Furthermore, anti-cortisol antibodies were immobilized on the gold surface. In this work, a lower envelope method was applied and the local maximum of the SPR signature was analyzed, presenting a sensitivity of 0.275 ± 0.028 nm/(ng/mL) for a concentration range from 0.1 to 10 ng/mL. In another study, Leitão et al. [19] proposed an SPR-based immunosensor for the detection of cortisol. In this work, an AuPd alloy-coated polymer optical fiber (POF) was treated chemically for the functionalization of the AuPd alloy with anti-cortisol antibodies. A sensitivity of 3.56 ± 0.20 nm/log(ng/mL) was attained in this work for an LOD of 0.001 ng/mL. Besides, Soares et al. [20] reported a silica optical fiber immunosensor with a D-shaped configuration for cortisol detection based on SPR. This standard single-mode fiber was coated with a gold nanofilm and functionalized with anti-cortisol antibodies. For a concentration range from 0.01 to 100 ng/mL, this immunosensor presented a logarithmic sensitivity of 0.65 ± 0.02 nm/log(ng/mL). Recently, Gomes et al. [21] developed a highly sensitive optical fiber immunosensors for cortisol detection and quantification in clinically and environmentally relevant concentration ranges below 5 ng/mL. The sensors rely on polyimide (PI)-based cavities forming Fabry-Pérot interferometer and on the Vernier effect induced by an additional in-series cavity formed after pulsed CO_2 laser-induced partial transformation of the polyimide into graphene. Finally, Arcadio et al. [22] reported an SPR biosensor based on POF via different functionalization protocols involving cysteamine and lipoic acid and demonstrating LODs of 0.8 pg/mL and 0.2 pg/mL, respectively, in a concentration range from 0.0001 to 0.1 ng/mL. Despite the good performance achieved at low concentration ranges, currently it is also desirable to have devices able to work over a wide concentration range covering up to hundreds of ng/mL to be better suited for various fish species. Moreover, it is also desirable to simplify as much as possible the procedures to functionalize the fiber surface.

In this context, the present work aims to develop and test a long period grating (LPG) coated with graphene oxide (GO) to develop a biosensor integrated into a flow cell for the detection of cortisol, as illustrated in Fig. 1. The LPG is fabricated into a double-clad fiber (DCF) with W-shaped refractive index (RI) profile and tuned to work in mode transition. The GO overlay straightly provides carboxyl functional groups on the sensor surface allowing the immobilization of the anti-cortisol antibody using EDC/NHS chemistry [23,24]. The advantages lie in the fact that the functionalization process is faster compared to the ones carried out in other studies, since an intermediate linker or another chemical step is not necessary. Moreover, the integration into a microfluidics system enables to control the temperature, to keep the fiber in constant strain state without bending, and to use lower amount of solutions, allowing the use of smaller volumes of reagents and chemicals. Cortisol detection tests were performed using cortisol concentrations ranging from 0.01 to 100 ng/mL in phosphate-buffered saline (PBS), achieving an LOD of 0.06 ng/mL. Therefore, the device stands out for good performance over a wide working range of concentrations of relevant interest. Finally, control tests for selectivity assessment were carried out using glucose and testosterone as the interfering substances in a sensor functionalized with anti-cortisol antibodies.

2. Materials and methods

2.1. Reagents

Hydrofluoric acid (HF), Sodium nitrate ($NaNO_3$), Potassium permanganate ($KMnO_4$), Sulfuric acid (H_2SO_4), and Hydrogen peroxide (H_2O_2) were supplied from Merck Life Science (Milano, Italy). N-(3-dimethylaminopropyl)-N'-ethylcarbodiimide hydrochloride (EDC) and N-hydroxysuccinimide (NHS, 98 %), were purchased from Thermo Fisher Scientific, USA. Bovin serum albumin (BSA), phosphate buffered saline (PBS) tablets (pH = 7.4), and ethanol absolute (≥99.8 %) were obtained from Fisher Scientific, USA. Deionized (DI) water was obtained from a Milli-Q water purification system and was used as received. Hydrocortisone (cortisol, ≥98 %), 17α-Methyltestosterone (testosterone, ≥97 %), and D-(+)-Glucose (glucose ≥99.5 %) were purchased from Sigma-Aldrich, Germany. The monoclonal anti-cortisol antibody was acquired from Randox, UK.

2.2. LPG fabrication

The fiber optic device proposed in this study comprises an LPG inscribed in an unconventional single-mode fiber employing double cladding with a W shaped RI profile, leveraging the mode transition effect. Specifically, the LPG transducers were inscribed into the S1310 fiber from Nufern, USA. The core and outer cladding diameters align with those of standard single-mode fiber, measuring 8 μm and 125 μm, respectively. Additionally, it features an inner cladding around 95 μm in diameter. Such a W shaped profile of the RI is created by using pure silica for the core and outer cladding, while the inner cladding is made from fluorine-doped glass, which lowers the silica RI. Additional specifications of the fiber include a core numerical aperture (NA) of 0.12 and a mode field diameter (MFD) of 10.4 ± 0.8 μm at a wavelength of 1.55 μm. The LPG inscription was carried out utilizing a platform employing the electric arc discharge (EAD) method, noted for its effectiveness on pure-silica core fibers and other non-photosensitive media. Detailed discussions of this technique are beyond the scope of this paper; however, comprehensive descriptions are available elsewhere [25]. In essence, the method consists of intermittently exposing the bare fiber to an electric arc formed between a pair of electrodes while applying tension to the fiber. This exposure induces localized RI alterations and minorly reshapes the fiber's geometry through tapering.

The W shaped structure of the fiber enabled specific cladding modes to propagate within the external cladding layer, preventing interaction with the core mode. However, by chemically etching the fiber (reducing the thickness of the outer cladding), the number of outer cladding modes

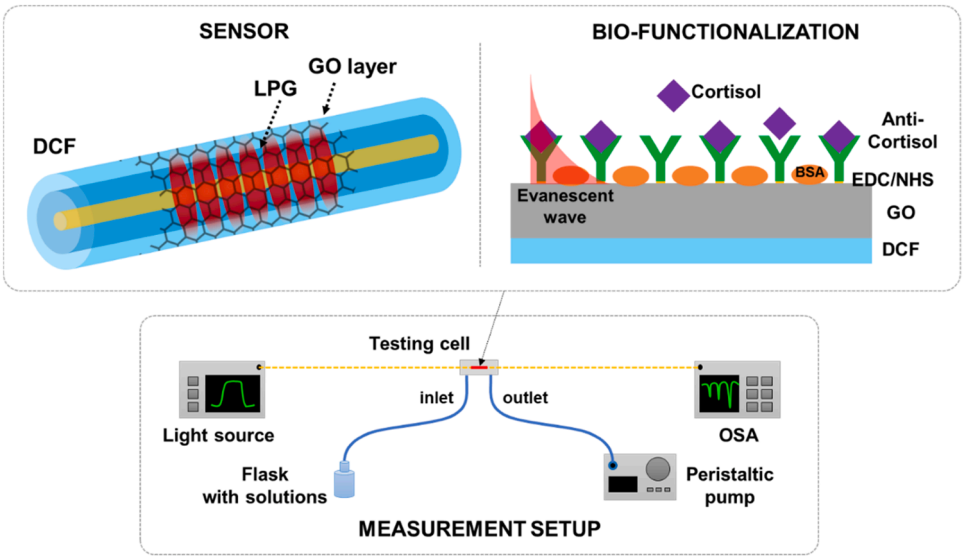

Fig. 1. Schematic picture of the developed immunosensor, including the schematics of GO coated LPG in DCF fiber, GO coated DCF surface prepared for the bio-assay to detect cortisol, and measurement setup.

decreased, i.e. a mode can move from the outer to inner cladding and, consequently, all cladding modes explored the transition phenomenon. During the mode transition a significant enhancement of the surrounding RI sensitivity was achieved. So far, the standard approach to induce the modal transition in LPGs relies on the use of standard SMF coated with high RI overly. Instead, the use of W-type DCF allowed maintaining band visibility, thereby improving resonance wavelength detection and signal-to-noise ratio [26].

The etched LPG is subsequently coated with a nano-sized overlay of graphene oxide, as illustrated schematically in Fig. 1.

2.3. Graphene oxide coating

Graphene oxide is an oxidized form of graphene produced through the oxidation and exfoliation of graphite, which introduces oxygen-containing functional groups such as carboxyl (-COOH), hydroxyl (-OH), and epoxy (-O-) onto the basal planes and edges. This is typically achieved via a modified Hummers' method [27,28]. In this study, a small amount of flake graphite (5 nm average particle size, 99.75 % purity, Asbury Carbons, USA) was stirred vigorously for five days in a solution of $NaNO_3$ and $KMnO_4$ within concentrated H_2SO_4. Afterward, the mixture was washed in a 5 % H_2SO_4 solution, followed by treatment with 30 % H_2O_2 to complete the oxidation process. Impurities and inorganic anions were removed through cycles of washing, centrifugation, and resuspension in a 3 % H_2SO_4 and 0.5 % H_2O_2 solution, enhanced by ultrasonication and stirring. To create the GO layer, 10 mg of the resulting powder was suspended in 5 mL of water via ultrasonication, then centrifuged at 14,000 rpm to remove larger particles.

The 1 mg/mL GO dispersion was then deposited onto the LPG surface through dip-coating, withdrawing at a speed of 300 mm/min and repeating this process 20 times (multi-dip approach).

The material has been characterized using Raman spectroscopy (Renishaw inVia, UK) and scanning electron microscopy (SEM, FEI Quanta 200 FEG) with energy-dispersive X-ray spectroscopy (EDX).

2.4. Experimental measurement setup

An *ad hoc* developed experimental setup (Fig. 1) was built up to characterize the fiber sensors and then to assess the biosensing performance. One end of the fibers was linked to a multi-LED light source (Fibrelabs, Inc., SLD1310/1430/1550/1690), while the other end was connected to a broadband optical spectrum analyzer (OSA) featuring a high optical resolution of 0.1 nm (Yokogawa, AQ6370D). A peristaltic pump (GILSON Minipulse 3) was employed to deliver liquid solutions at controlled rates. Additionally, a personal computer equipped with a custom-developed CVI-Windows software program was connected to the OSA via Ethernet, allowing for the recording and processing of the optical signals from the LPG-based sensors with enhanced detection accuracy and precision at the level of 10^{-3} nm. Further details can be found in prior publications [16,29].

2.5. GO coated LPG functionalization

The functionalization with anti-cortisol antibodies is a crucial step for specificity to cortisol and is schematically depicted in Fig. 1. Anti-cortisol antibodies were immobilized onto the cladding surface of LPGs. To favorite the antibody linking, the fiber surface was coated with GO. The GO film provided carboxyl functional groups which, through surface activation via EDC/NHS chemistry, allowed us to directly graft the specific antibody onto the fiber [23,24]. Therefore, the first step of the functionalization consisted in injecting a solution of EDC/NHS (0.2 M/0.5 M in PBS) for 30 min at a flow rate of 37.5 µL/min. This step is crucial for the correct and effective activation of the carboxyl groups. Afterwards, the anti-cortisol antibody (500 µg/mL prepared in PBS) was injected into the microfluidic cell for 1 h at a flow rate of 12.5 µL/min for covalent immobilization. Then, the fiber surface was washed with PBS at a flow rate of 125 µL/min for 5 min to remove the unbounded antibodies and, consequently, it was passivated with BSA solution (10 mg/mL) for 20 min at a flow rate of 37.5 µL/min, to prevent from non-specific bindings. Lastly, PBS was injected at a flow rate of 125 µL/min for 5 min and the flow stopped for 5 min corresponding to the measuring window of the blank solution.

2.6. Measuring protocol: cortisol detection and selectivity test

For the cortisol detection tests in PBS, five cortisol concentrations were used, namely 0.01, 0.1, 1, 10, and 100 ng/mL. Firstly, a stock solution (0.1 mg/mL) was prepared using cortisol diluted in 1 % of ethanol and 99 % of PBS. Then, the five cortisol concentrations were prepared through consecutive dilutions of the stock solution using PBS.

The measurement procedure involved injecting the cortisol solutions into the flow cell for 30 min at a flow rate of 25 µL/min. After each concentration, a washing step with PBS was conducted for 5 min at a flow rate of 125 µL/min, followed by a 5 min pause to allow for

measurements. This procedure was repeated for each cortisol concentration.

The operating principle of the immunosensor was based on the monitoring of the interaction between the biological recognition element or bio-receptor (anti-cortisol antibody, in this case) grafted onto the functionalized surface of the fiber and the specific target analyte (cortisol, in this case). This binding interaction induced changes in both the thickness and RI of the sensing bio-layer, thus generating in turn a shift of the LPG resonance wavelength toward shorter wavelengths which determined an increase in the effective RI of cladding modes according to LPG working principle [23]. Selectivity tests for cortisol were also evaluated, using glucose and testosterone as the control tests. Therefore, anti-cortisol antibodies were also immobilized on the sensor surface following the functionalization protocol described in Section 2.5 and tested for 1 ng/mL of glucose, testosterone, and cortisol. These concentrations were prepared through consecutive dilutions of a stock solution using PBS, as the cortisol one. The measuring protocol followed the one previously described.

2.7. LPG numerical analysis

A simulation environment was custom developed to obtain LPG spectra and designing the transducer. It employed the model proposed by Anemogiannis et al. [30], as suitable tool to describe the light propagation in multi-layer optical fiber with any azimuthal profile combined with the coupled-mode theory. This approach, widely discussed in [31,32] and more recently by the authors in [23,24,33], was selected because it allows to study grating with a slowly varying RI of the core/cladding and/or geometrical features along the length of the fiber. Starting from the fiber and grating parameters, the model allowed the calculation of effective RIs and electric field profiles of the modes, mode coupling coefficients and, finally, transmitted spectra of the LPG in multi-cladding fiber. The dispersion of fiber materials as a function of the operating wavelength has also been considered. Specifically, we focused the attention on approximated LP modes and, since it was assumed that the RI change is azimuthally symmetric, only azimuthally symmetric modes LP_{0i} were considered. It is well assessed that LP approximation is still considered valid in the case of optical fiber coated with high RI overlay [31,32] and so, we considered it still valid. Finally, concerning the grating features, we assumed it to have a sinusoidal profile in the fiber core, where RI changes had an amplitude of $1.5 \bullet 10^{-4}$ and a periodicity $\Lambda = 400$ μm.

3. Results and discussion

3.1. GO characterization

The structure of GO prepared according to Section 2.3, was examined with Raman spectroscopy, and the spectrum of a GO film on a glass substrate, shown in Fig. 2(a), revealed significant peaks: the D band at about 1340 cm^{-1}, indicating structural defects from oxygen group attachments on the carbon basal plane; the G band around 1580 cm^{-1}, related to first-order E_2g phonon mode scattering of sp^2-bonded carbon atoms; a smaller 2D band at 2687 cm^{-1}; and combined D+G and 2G bands at 2933 cm^{-1} and 3191 cm^{-1}, respectively [34].

SEM was used to observe the GO's nanostructure on the optical fiber. The SEM image at 10,000x magnification, as shown in Fig. 2(b), displays GO's multi-layered lamellar structure, with visible edges of individual sheets and wrinkled areas where the films stack together. Moreover, EDX analysis the presence of atomic% of C > 65 %, O > 20 %, Si ~ 10 %, S and Na < 1 %.

3.2. Simulation of fiber modes in DCF

By using the simulation tool described in Section 2.7 [23,33,35] together with DCF parameters mentioned in Section 2.2, it is possible to achieve the LPG transmitted spectra during each fabrication step.

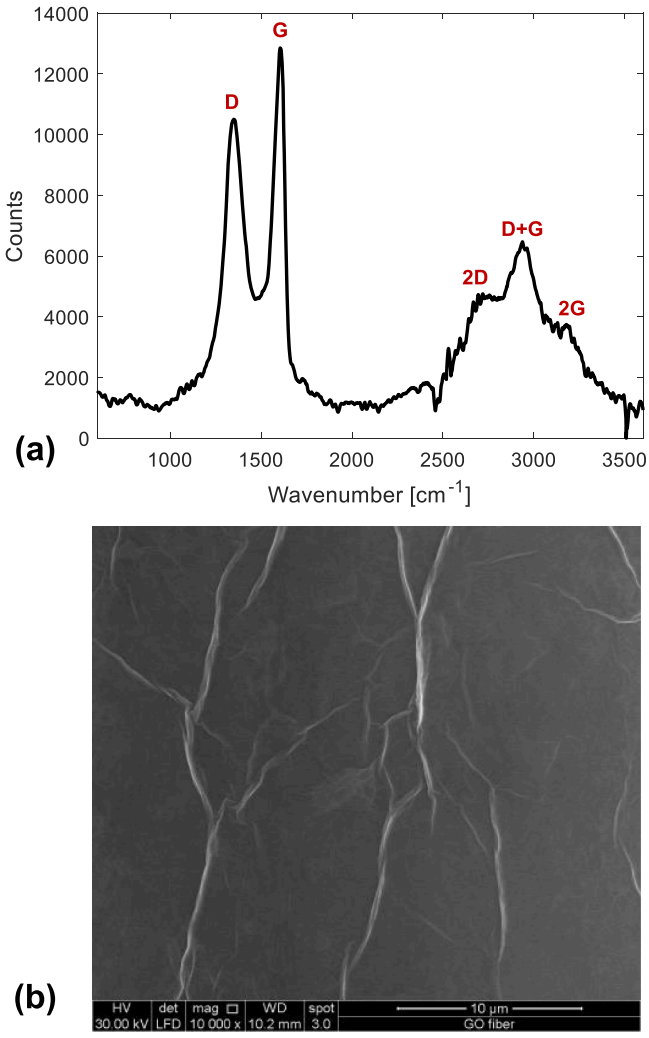

Fig. 2. (a) Graphene oxide's Raman spectrum observed on a glass substrate; (b) SEM micrograph displaying graphene oxide deposition on an optical fiber.

Here, we focus the attention on electric field distributions of different cladding/core modes to show the modal transition phenomena in such kind of fiber. Fig. 3 illustrates the normalized electric field profiles for the first eight LP_{0i} modes for $\lambda = 1550$ nm, where the fiber regions were marked using dashed lines for better visualization. Here, only one mode, LP_{01}, is confined in the core region (core-mode) with an effective RI of 1.4410. Moreover, there are two modes, LP_{02} and LP_{03}, which are guided into the ring-shaped outer cladding exhibiting effective RIs higher than the core-mode, i.e. 1.4433 and 1.4413, respectively. Following, higher order modes LP_{04} to LP_{08}, behave as standard cladding modes having significant electrical field in the whole fiber structure. Decreasing the thickness of ring-shaped outer cladding, the number of modes therein confined decreases giving rise to the mode transition [26].

These inputs were employed for the simulation of LPG full spectra for a direct comparison with the experimental results during fabrication steps, for the tuning of the working point within the mode transition region in turn experiencing higher SRI sensitivity. As a matter of fact, the details and results of further simulations are reported in the following Section 3.3 comparatively with experimental data.

3.3. LPG sensor

To fine-tune the characteristics of the LPG, it is crucial to select the

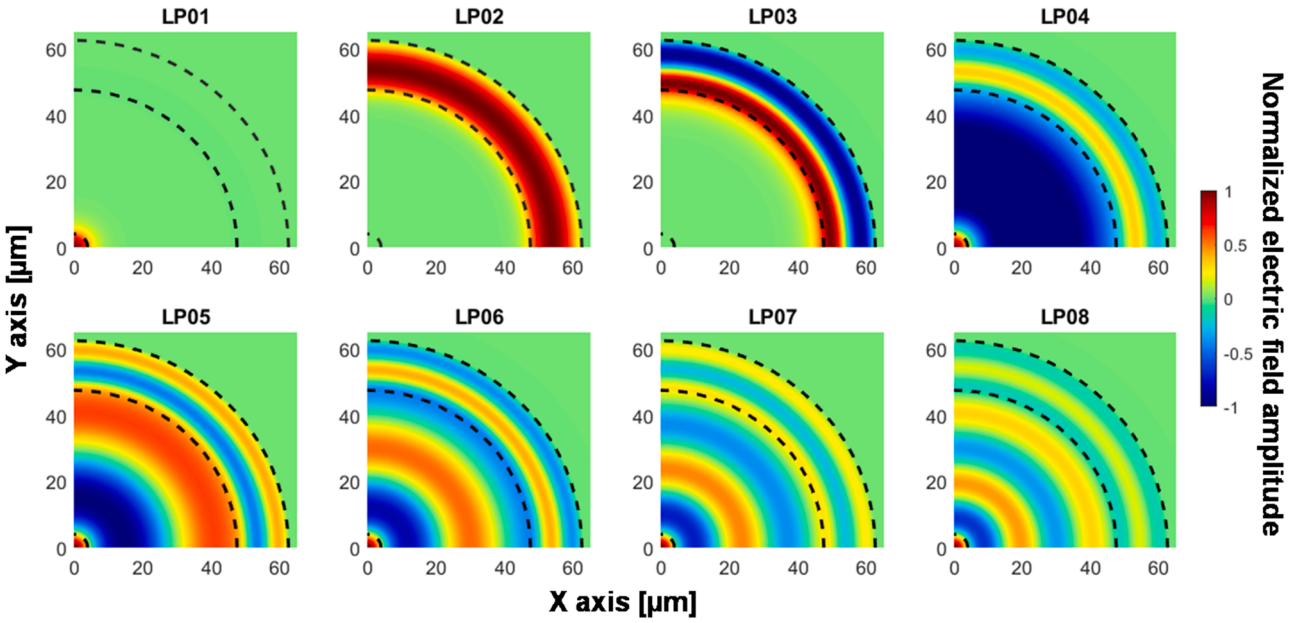

Fig. 3. Normalized electric field profile of the first eight azimuthally symmetric LP_{0i} fiber modes in DCF with W-shaped profile at $\lambda = 1550$ nm. The fiber regions are marked with dashed lines.

proper inscription parameters. In this case, a single perturbation was introduced by exposing the fiber to an electric arc for 700 ms at a power level of 20 steps (a proprietary value by Sumitomo, Japan) between the electrodes of a fusion splicer, with a 0.8 mm gap between the tips. To maintain the fiber steadily aligned, a 12 g weight was attached to the same. This process was repeated at regular intervals, with a period (Λ) of 400 μm selected. This setting enabled the excitation of cladding modes of 5th and 6th orders across the wavelength range of 1200–1650 nm. This design was further substantiated by numerical simulations. An illustrative example of device transmitted spectrum measured with the setup described in Section 2.4 is shown in Fig. 4(a). The figure displays two primary resonance dips, positioned at 1230 nm (linked to the 5th order mode or LP_{06}, in the following λ_5) and 1375 nm (corresponding to the 6th or LP_{07}, in the following λ_6). In the same picture, the numerically simulated spectrum achieved following results from Section 3.2 is also graphed with a dotted line showing a good agreement. The bulk RI sensitivity of the grating was evaluated by immersing it in liquids with precisely calibrated RIs. A sensitivity of about −80 nm/RIU was determined through a linear approximation over the RI range of 1.33 to 1.37 for the λ_6 band. Such sensitivity value is too low for any biosensing purpose [36].

Adjusting the working point of the LPG within the transition zone requires control of the outer cladding diameter through wet chemical etching, a process detailed in [26]. In short, the grating was etched using a 24 % v/v HF solution, yielding an etch rate around 0.6 μm/min. The device spectrum was continuously acquired throughout the etching. Fig. 4(b) and 4(c) show the evolution of resonance wavelength and amplitude of the resonance dips, respectively, with diameter reduction (from right to left). Markers highlight changes in attenuation bands for the 4th, 5th, and 6th order cladding modes. Additionally, numerical simulations are included as dotted lines, showing good alignment with the experimental results. The etching predominantly caused the attenuation band resonances to shift towards longer wavelengths and an overall increase in their peak depth. Notably, as the diameter neared the values corresponding to mode transitions, the rate of shift remarkably increased [26,32] and, in turn, the experimental resonance amplitudes experienced a decrease (anyway the band remained well visible). For a diameter decrease of about 5 μm, the 6th mode started experiencing a transition, however unfortunately the band became poorly visible at that point, so the etching was continued, and attention focused on the 5th mode afterwards. Specifically, at a diameter decrease of about 9 μm, a distinct transition was observed from the 5th mode attenuation band to the 6th mode. As the diameter decreased further, the 4th mode band, shifting to longer wavelengths, became discernible within the spectrum range under investigation. Additionally, as the diameter decreased by approximately 17 μm, the band of the 5th mode started moving toward the expected location of the next, 7th mode (which was outside the observable wavelength range). At this stage, the etching process was stopped to fix the LPG at its maximum sensitivity, establishing the sensor's final operating point.

The spectra of the LPG after etching, while immersed in water, are shown in Fig. 5. Initial focus was placed on the attenuation band at 1580 nm with an 18 dB depth (this band was out of the interrogation range when measured in air). Additional samples were prepared in a similar manner to assess the repeatability and reproducibility of the results [37]. To evaluate the influence of etching on sensitivity, we observed the responses of the LPG in solutions with a RI between 1.33 and 1.37. After etching, the sensitivity increased significantly up to −1400 nm/RIU, highlighting the deliberate choice of the working point within the mode transition area through the etching process.

After the etching procedure, the gratings were covered with a 20 nm layer of graphene oxide, utilizing the technique outlined in Section 2.3. This application aimed to incorporate carboxyl functional groups onto the surface of the fiber. As depicted in Fig. 6, this GO deposition caused a 30 nm blue shift in the resonance wavelengths moving it near to 1550 nm when the gratings were submerged in water. This shift was attributed to the high RI of GO ranging in 1.8–2.0 [24], increasing the effective RIs of cladding modes. Finally, it is worth highlighting that, despite the GO's inherent absorption losses which led to an overall decrease in the peak visibility, the depth of the resonance peak consistently remained above 13 dB. In the same picture, the numerical spectra before and after GO deposition are also reported with a dotted line demonstrating a satisfactory agreement.

3.4. Cortisol detection

To assess the response of the LPG-GO immunosensors to cortisol, different concentrations of cortisol solution in PBS ranging from 0.01 ng/mL to 100 ng/mL were tested. Fig. 6 illustrates the dose-response curve representing the changes in wavelength ($\Delta\lambda_{LPG}$) relative to the

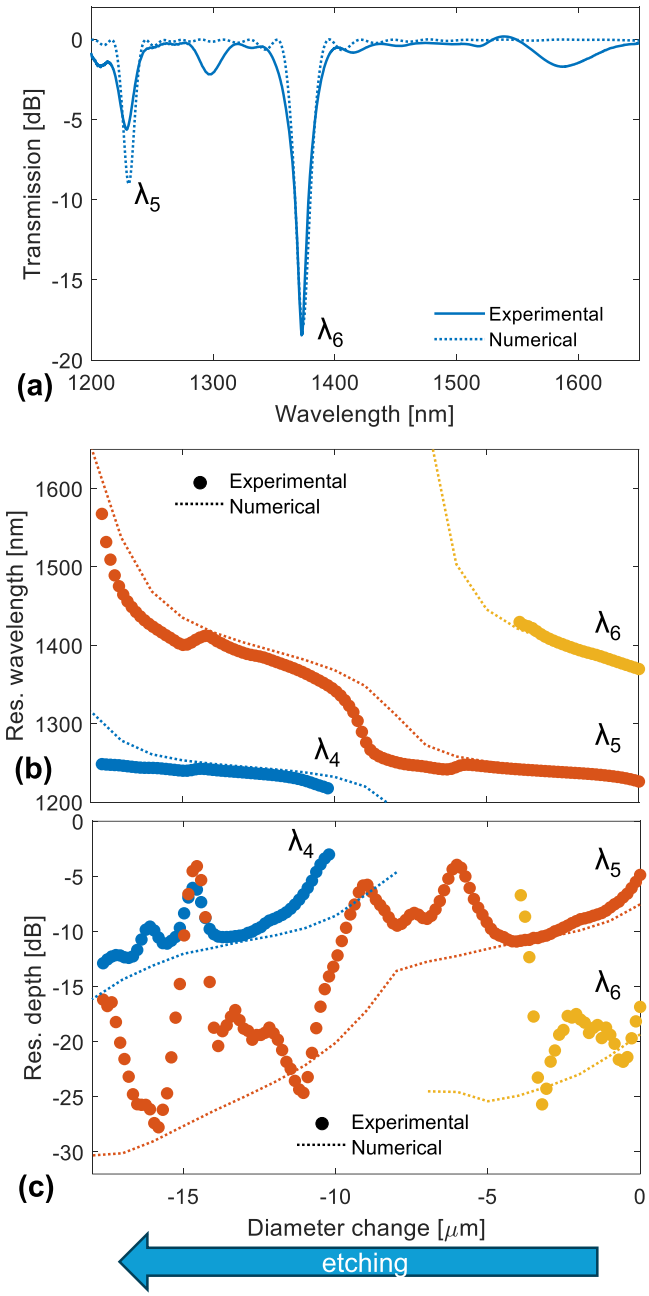

Fig. 4. (a) Transmission spectrum of the LPG (solid line) after fabrication (before etching) and comparison with numerical simulated spectrum (dotted). Influence of fiber diameter variation throughout the etching process on the resonance wavelengths (b) and intensities (c) of the 6th, 5th, and 4th order cladding modes. Markers represent experimental data, while corresponding numerical results are illustrated with dotted lines in matching colors.

blank solution, plotted against the cortisol concentration. Additionally, the figure includes the Hill fitting of the experimental data along with the associated error bars. The error bars were calculated as the maximum standard deviation obtained in three independent measurements considering three distinct immunosensors prepared according to previous description, thus providing a very reliable and effective way of assessing the reproducibility [37]. Specifically, the results can be modeled by the Hill equation (Eq. (1)), a mathematical model that reflects the interaction between the specific antibody and the analyte [38], also considering the saturation phenomenon. The Hill equation is expressed as follows:

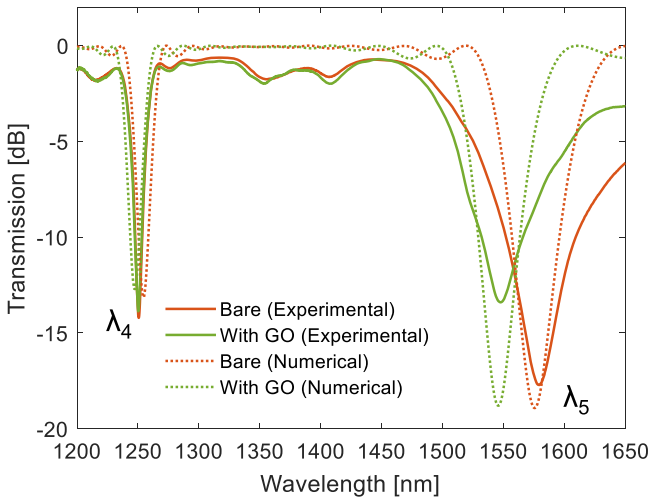

Fig. 5. Transmission spectra of the LPG when water is the outer medium: after etching (red) and after GO deposition (green). The experimental values are reported with solid lines whereas the numerical results with dotted ones.

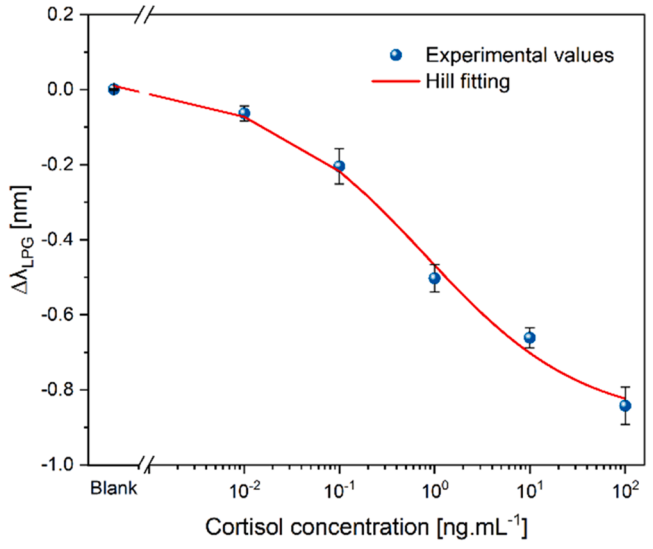

Fig. 6. Resonant wavelength changes as a function of cortisol concentration (dose-response curve) and Hill fitting of the experimental values.

$$\Delta\lambda_c = \lambda_c - \lambda_0 = f(c) = \Delta\lambda_{max}\cdot\frac{c^n}{K^n + c^n} \quad (1)$$

where c indicates the cortisol concentration, λ_c and λ_0 denote the wavelength at concentration c and blank, respectively; $\Delta\lambda_{max}$ is calculated as the difference between the resonance wavelength at the saturation level and that of the blank solution. Typically, the parameters n and K represent the constants used in the Hill fitting analysis, in which n refers to the Hill coefficient, describing the cooperativity of ligand binding, and K is a constant related to the affinity between anti-cortisol antibodies and cortisol antigens. The parameters for the Hill fitting are presented in Table 1.

Table 1
Hill fitting parameters associated with the response of LPG-GO to cortisol in PBS.

$\Delta\lambda_{max}$ [nm]		K [ng/mL]		n		Statistics	
Value	St. error	Value	St. error	Value	St. error	$\chi 2$	R^2
−0.91	0.19	0.65	0.66	0.46	0.30	0.0033	0.97

According to [37], if a full calibration curve of the biosensor is attained, LOD can be obtained from the calibration curve and calculated as follows:

$$c_{LOD} = f^{-1}(f(0) + 3\sigma_{max}) \quad (2)$$

where f^{-1} is the inverse of the Hill function f defined in Eq. (1), $f(0)$ is the value of the blank signal, and $3\sigma_{max}$ the maximum standard deviation obtained among all the experimental points. Therefore, it was obtained a LOD of 0.06 ng/mL for σ_{max} of 0.05 nm.

Another important parameter to assess the biosensing performance is the surface sensitivity at low concentrations ($S_{low\ c}$). When $c << K$, Eq. (1) can be re-written as:

$$\Delta\lambda_c = \lambda_c - \lambda_0 = f(c) = \Delta\lambda_{max} \cdot \frac{c^n}{K^n + c^n} \approx \Delta\lambda_{max} \cdot \frac{c^n}{K^n} \quad (3)$$

and hence the surface sensitivity becomes as in Eq. (4):

$$S_{low\ c} = n \cdot \Delta\lambda_{max} \cdot \frac{c^{n-1}}{K^n} \quad (4)$$

Therefore, $S_{low\ c}$ can be calculated using the last equation and the fitting parameters gathered in Table 1. Specifically, when c ranges between 10^{-2} and 10^{-1} ng/mL, a surface sensitivity of 1.7 nm/(ng/mL) was retrieved.

3.5. Evaluation of the stability

The stability of the optical signal of LPG-GO immunosensors (i.e., λ_{LPG}) over a long-term period was also taken in consideration. In fact, this parameter is crucial for assessing the sensor accuracy and precision in the detection [37]. Fig. 7 accounts for an example of the spectral evolution of λ_{LPG} scaled down to 0 ($\Delta\lambda_{LPG}$) as a function of the time by keeping the immunosensor in PBS environment under controlled thermal and mechanical conditions for several hours. Remarkably, it should be underlined that the mean deviation of the $\Delta\lambda_{LPG}$ was 0.015 nm, while the maximum (or peak-to-peak) deviation was just 0.068 nm, values which are comparable with σ_{max} (0.05 nm) retrieved from the dose-response curve of Fig. 6.

3.6. Evaluation of the selectivity

The selectivity of the LPG-GO immunosensor for cortisol was tested using possible interfering substances, including testosterone and glucose (both at a concentration of 1 ng/mL). For the same concentration (1 ng/mL), the results presented in Fig. 8 show that this immunosensor response was not affected by testosterone (green) and glucose (red),

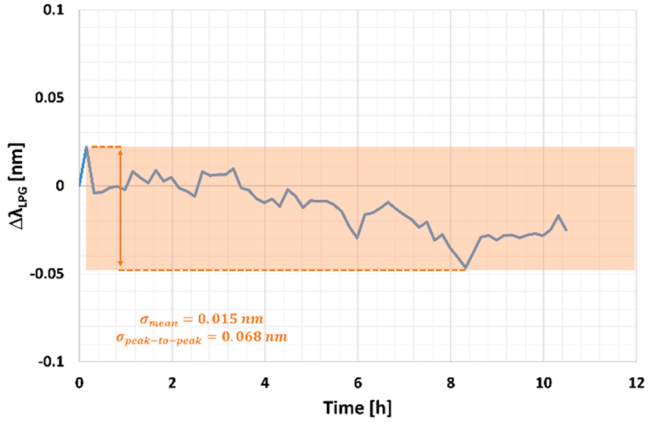

Fig. 7. Stability of the LPG optical signal scaled down to 0 (i.e., $\Delta\lambda_{LPG}$) as a function of the time over hours when the sensor is placed in PBS environment at controlled thermal and mechanical conditions.

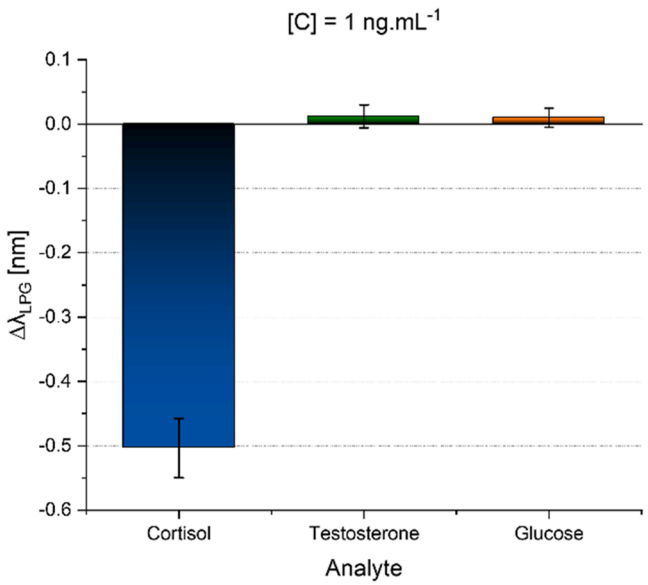

Fig. 8. Selectivity test using interfering substances (testosterone and glucose) and the analyte (cortisol) at 1 ng/mL.

since the wavelength shift was much higher for cortisol (blue) than for both the interfering substances tested (within the error bars).

4. Conclusion

This study successfully demonstrated the development of a graphene oxide-coated long period fiber grating immunosensor for the detection of cortisol, addressing a critical gap in aquaculture monitoring. The immunosensor, functionalized with anti-cortisol antibodies grafted into the sensing surface via one step process involving graphene oxide, exhibited a reliable detection range from 0.01 ng/mL to 100 ng/mL, with a notable LOD of 0.06 ng/mL, a value below the one required in normal conditions of healthy aquaculture environments. It is worth pointing out that both working range and LOD of the proposed technological platform are relevant for a vast class of fish species. Furthermore, the sensor showed good selectivity against potential interfering substances, such as testosterone and glucose. This innovation holds great promise for improving the real-time monitoring of fish welfare in RAS, potentially enhancing stress management, growth performance, and overall fish health. The integration of this technology could help optimize aquaculture operations and better support the rising demand for sustainable fish production. Future work should focus on the miniaturization and simplification of read-out systems, as well as permitting non-expert operators to perform the measurements in real scenario like in RAS units. This would pave the way to realize a portable platform using this technology, and hence to include it in a RAS tank installation to perform direct measurements in RAS water.

Disclosures

The authors declare no conflicts of interest.

CRediT authorship contribution statement

Simone Soares: Writing – original draft, Methodology, Investigation. **Ambra Giannetti:** Writing – review & editing, Resources, Methodology, Investigation. **Flavio Esposito:** Writing – original draft, Investigation, Conceptualization. **Lucia Sansone:** Writing – review & editing, Resources, Investigation. **Anubhav Srivastava:** Investigation. **Stefania Campopiano:** Supervision, Conceptualization. **Michele Giordano:** Supervision, Investigation. **Margarida Facão:** Writing –

review & editing, Investigation. **Nuno F. Santos:** Writing – review & editing, Supervision. **Agostino Iadicicco:** Writing – review & editing, Supervision, Conceptualization. **Carlos Marques:** Validation, Supervision, Resources, Project administration, Methodology, Conceptualization. **Francesco Chiavaioli:** Writing – review & editing, Validation, Supervision, Data curation, Conceptualization.

Declaration of competing interest

The authors declare that they have no known competing financial interests or personal relationships that could have appeared to influence the work reported in this paper.

Acknowledgments

This work was performed within the project "Monitoring of Honeybee Immunomodulation and Resilience to Stress Factors by Fiber Optic Technology" (MoBeeFO) CUP I53D23000390006 under PRIN 2022 grant financed by the European Union – Next Generation EU, Mission 4 Component 1 and Italian Ministry of University and Research. The research was co-funded by the financial support of the European Union under the REFRESH – Research Excellence For REgion Sustainability and High-tech Industries project number CZ.10.03.01/00/22003/0000048 via the Operational Programme Just Transition. This work was also supported by the Ministry of Education, Youth, and Sports of the Czech Republic conducted by the VSB-Technical University of Ostrava, under grant no SP2024/081. This work was developed within the scope of the projects CICECO (LA/P/0006/2020, UIDB/50011/2020 & UIDP/50011/2020) and DigiAqua (PTDC/EEI-EEE/0415/2021), financed by national funds through the Portuguese Science and Technology Foundation/MCTES (FCT I.P.). Simone Soares acknowledges FCT/MCTES for the PhD fellowship grant UI/BD/153066/2022. N. F. Santos acknowledges FCT I.P. for the research action 2022.04595.CEECIND (GraFiberSens project).

Data availability

Data underlying the results presented in this paper are not publicly available at this time but may be obtained from the authors upon reasonable request.

References

[1] C.E. Boyd, Aquaculture. Freshwater, Elsevier Inc., 2013, https://doi.org/10.1016/b978-0-12-409548-9.03764-7.
[2] H.O. Halvorson, R. Smolowitz, Aquaculture, Appl. Microbiol. Agro/Food (2009) 17–22.
[3] S. Balami, Recirculation aquaculture systems: components, advantages, and drawbacks, Trop. Agroecosystems 2 (2021) 104–109, https://doi.org/10.26480/taec.02.2021.104.109.
[4] A.B. Holan, C. Good, M.D. Powell, Health Management in Recirculating Aquaculture Systems (RAS), Elsevier Inc., 2020, https://doi.org/10.1016/b978-0-12-813359-0.00009-9.
[5] K. Ogawa, F. Ito, M. Nagae, T. Nishimura, M. Yamaguchi, A. Ishimatsu, Effects of acid stress on reproductive functions in immature Carp, Cyprimus Carpio, Water, Air, Soil Pollut 130 (2001) 887–892, https://doi.org/10.1023/A:1013803517375.
[6] E. Fanouraki, N. Papandroulakis, T. Ellis, C.C. Mylonas, A.P. Scott, M. Pavlidis, Water cortisol is a reliable indicator of stress in European sea bass, Dicentrarchus labrax, Behaviour 145 (2008) 1267–1281, https://doi.org/10.1163/156853908785765818.
[7] V.C. Mota, C.I.M. Martins, E.H. Edinga, A.V.M. Canário, J.A.J. Verretha, Steroids accumulate in the rearing water of commercial recirculating aquaculture systems, Aquac. Eng. 62 (2014) 9–16, https://doi.org/10.1016/j.aquaeng.2014.07.004.
[8] D. Aguiar, C. Marques, A.C. Pereira, The importance of monitoring cortisol in the agri-food sector—A systematic review, Metabolites 13 (2023) 1–14, https://doi.org/10.3390/metabo13060692.
[9] A. Tintos, J.M. Míguez, J.M. Mancera, J.L. Soengas, Development of a microtitre plate indirect ELISA for measuring cortisol in teleosts, and evaluation of stress responses in rainbow trout and gilthead sea bream, J. Fish Biol. 68 (2006) 251–263, https://doi.org/10.1111/j.0022-1112.2006.00898.x.
[10] L. Zu, X. Wang, P. Liu, J. Xie, X. Zhang, W. Liu, Z. Li, S. Zhang, K. Li, A. Giannetti, W. Bi, F. Chiavaioli, L. Shi, T. Guo, Ultrasensitive and multiple biomarker discrimination for Alzheimer's disease via plasmonic & microfluidic sensing technologies, Adv. Sci. 11 (2024) 2308783, https://doi.org/10.1002/advs.202308783.
[11] S. Cao, R. Chen, Q. Yang, X. He, F. Chiavaioli, Y. Ran, B.-O. Guan, Point-of-care diagnosis of pre-eclampsia based on microfiber Bragg grating biosensor, Biosens. Bioelectron. 249 (2024) 116014, https://doi.org/10.1016/j.bios.2024.116014.
[12] C. Caucheteur, J. Villatoro, F. Liu, M. Loyez, T. Guo, J. Albert, Mode-division and spatial-division optical fiber sensors, Adv. Opt. Photonics. 14 (2022) 1–86, https://doi.org/10.1364/AOP.444261.
[13] M. Lobry, M. Loyez, M. Debliquy, K. Chah, E. Goormaghtigh, C. Caucheteur, Electro-plasmonic-assisted biosensing of proteins and cells at the surface of optical fiber, Biosens. Bioelectron. 220 (2023) 114867, https://doi.org/10.1016/j.bios.2022.114867.
[14] M. Loyez, M. Adolphson, J. Liao, L. Yang, From whispering gallery mode resonators to biochemical sensors, ACS Sensors 8 (2023) 2440–2470, https://doi.org/10.1021/acssensors.2c02876.
[15] M. Loyez, E.M. Hassan, M. Lobry, F. Liu, C. Caucheteur, R. Wattiez, M.C. DeRosa, W.G. Willmore, J. Albert, Rapid detection of circulating breast cancer cells using a multiresonant optical fiber aptasensor with plasmonic amplification, ACS Sensors 5 (2020) 454–463, https://doi.org/10.1021/acssensors.9b02155.
[16] I. Del Villar, E. Gonzalez-Valencia, N. Kwietniewski, D. Burnat, D. Armas, E. Pituła, M. Janik, I.R. Matías, A. Giannetti, P. Torres, F. Chiavaioli, M. Śmietana, Nanophotonic crystal dshaped fiber devices for label-free biosensing at the attomolar limit of detection, Adv. Sci (2024) 2310118, https://doi.org/10.1002/advs.202310118.
[17] N. Cennamo, L. Pasquardini, F. Arcadio, L. Zeni, Pollen-based natural nanostructures to realize nanoplasmonic biochips for single-molecule detection, Sensors Actuators B Chem (2024) 136404, https://doi.org/10.1016/j.snb.2024.136404.
[18] C. Leitao, S.O. Pereira, N. Alberto, M. Lobry, M. Loyez, F.M. Costa, J.L. Pinto, C. Caucheteur, C. Marques, Cortisol in-fiber ultrasensitive plasmonic immunosensing, IEEE Sens. J 21 (2021) 3028–3034, https://doi.org/10.1109/JSEN.2020.3025456.
[19] C. Leitão, A. Leal-Junior, A.R. Almeida, S.O. Pereira, F.M. Costa, J.L. Pinto, C. Marques, Cortisol AuPd plasmonic unclad POF biosensor, Biotechnol. Reports 29 (2021) 1–6, https://doi.org/10.1016/j.btre.2021.e00587.
[20] M.S. Soares, L.C.B. Silva, M. Vidal, M. Loyez, M. Facão, C. Caucheteur, M.E. V. Segatto, F.M. Costa, C. Leitão, S.O. Pereira, N.F. Santos, C.A.F. Marques, Label-free plasmonic immunosensor for cortisol detection in a d-shaped optical fiber, Biomed. Opt. Express. 13 (2022) 1–16, https://doi.org/10.1364/boe.456253.
[21] H.C. Gomes, X. Liu, A. Fernandes, C. Moreirinha, R. Singh, S. Kumar, F. Costa, N. Santos, C. Marques, Laser-Induced graphene-based Fabry-Pérot cavity label-free immunosensors for the quantification of cortisol, Sensors Actuat. Reports 7 (2024) 100186, https://doi.org/10.1016/j.snr.2024.100186.
[22] F. Arcadio, S. Soares, J. Nedoma, D. Aguiar, A.C. Pereira, L. Zeni, N. Cennamo, C. Marques, POF-based biosensors for cortisol detection in seawater as a tool for aquaculture systems, Sci. Rep. 14 (2024) 13117, https://doi.org/10.1038/s41598-024-63870-7.
[23] F. Esposito, L. Sansone, A. Srivastava, F. Baldini, S. Campopiano, F. Chiavaioli, M. Giordano, A. Giannetti, A. Iadicicco, Long period grating in double cladding fiber coated with graphene oxide as high-performance optical platform for biosensing, Biosens. Bioelectron. 172 (2021) 112747, https://doi.org/10.1016/j.bios.2020.112747.
[24] F. Esposito, L. Sansone, A. Srivastava, A.M. Cusano, S. Campopiano, M. Giordano, A. Iadicicco, Label-free detection of vitamin D by optical biosensing based on long period fiber grating, Sensors Actuators B Chem 347 (2021) 130637, https://doi.org/10.1016/j.snb.2021.130637.
[25] F. Esposito, R. Ranjan, S. Campopiano, A. Iadicicco, Arc-induced long period gratings from standard to polarization-maintaining and photonic crystal fibers, Sensors 18 (2018) 918, https://doi.org/10.3390/s18030918.
[26] F. Esposito, A. Srivastava, L. Sansone, M. Giordano, S. Campopiano, A. Iadicicco, Sensitivity enhancement in long period gratings by mode transition in uncoated double cladding fibers, IEEE Sens. J. 20 (2020) 234–241, https://doi.org/10.1109/JSEN.2019.2942639.
[27] W.S. Hummers, R.E. Offeman, Preparation of graphitic oxide, J. Am. Chem. Soc. 80 (1958) 1339, https://doi.org/10.1021/ja01539a017.
[28] J.P. Rourke, P.A. Pandey, J.J. Moore, M. Bates, I.A. Kinloch, R.J. Young, N. R. Wilson, The real graphene oxide revealed: stripping the oxidative debris from the graphene-like sheets, Angew. Chemie Int. Ed. 50 (2011) 3173–3177, https://doi.org/10.1002/anie.201007520.
[29] F. Chiavaioli, D. Santano Rivero, I. Del Villar, A.B. Socorro-Leránoz, X. Zhang, K. Li, E. Santamaría, J. Fernández-Irigoyen, F. Baldini, D.L.A. van den Hove, L. Shi, W. Bi, T. Guo, A. Giannetti, I.R. Matias, Ultrahigh sensitive detection of tau protein as Alzheimer's biomarker via microfluidics and nanofunctionalized optical fiber sensors, Adv. Photonics Res. 3 (2022) 2200044, https://doi.org/10.1002/adpr.202200044.
[30] E. Anemogiannis, E.N. Glytsis, T.K. Gaylord, Transmission characteristics of long-period fiber gratings having arbitrary azimuthal/radial refractive index variations, J. Light. Technol. 21 (2003) 218–227, https://doi.org/10.1109/JLT.2003.808637.
[31] I. Del Villar, I. Matías, F. Arregui, P. Lalanne, Optimization of sensitivity in Long Period Fiber Gratings with overlay deposition, Opt. Express. 13 (2005) 56–69, https://doi.org/10.1364/OPEX.13.000056.
[32] A. Cusano, A. Iadicicco, P. Pilla, L. Contessa, S. Campopiano, A. Cutolo, M. Giordano, Mode transition in high refractive index coated long period gratings, Opt. Express. 14 (2006) 19–34, https://doi.org/10.1364/OPEX.14.000019.
[33] F. Esposito, L. Sansone, C. Taddei, S. Campopiano, M. Giordano, A. Iadicicco, Ultrasensitive biosensor based on long period grating coated with polycarbonate-

graphene oxide multilayer, Sensors Actuators B Chem 274 (2018) 517–526, https://doi.org/10.1016/j.snb.2018.08.002.
[34] Y. Zhu, S. Murali, W. Cai, X. Li, J.W. Suk, J.R. Potts, R.S. Ruoff, Graphene and graphene oxide: synthesis, properties, and applications, Adv. Mater. 22 (2010) 3906–3924, https://doi.org/10.1002/adma.201001068.
[35] K. Xu, Silicon MOS optoelectronic micro-nano structure based on reverse-biased PN junction, Phys. Status Solidi. (2019) 216, https://doi.org/10.1002/pssa.201800868.
[36] L. Sansone, S. Campopiano, M. Pannico, M. Giordano, P. Musto, A. Iadicicco, Photonic bandgap influence on the SERS effect in metal-dielectric colloidal crystals optical fiber probe, Sensors Actuators B Chem 345 (2021) 130149, https://doi.org/10.1016/j.snb.2021.130149.
[37] F. Chiavaioli, C. Gouveia, P. Jorge, F. Baldini, Towards a uniform metrological assessment of grating-based optical fiber sensors: from refractometers to biosensors, Biosensors (Basel) 7 (2017) 23, https://doi.org/10.3390/bios7020023.
[38] H. Moulahoum, F. Ghorbanizamani, The LOD paradox: when lower isn't always better in biosensor research and development, Biosens. Bioelectron. 264 (2024) 116670, https://doi.org/10.1016/j.bios.2024.116670.